65B Solid solutions

No. 65B-1 $(CH_3)_3NCH_2COO \cdot H_3PO_4$–$(CH_3)_3NCH_2COO \cdot H_3AsO_4$ (BP–BA)

1b	Θ vs. x phase diagram for $(CH_3)_3NCH_2COO \cdot H_3(P_{1-x}As_x)O_4$: Fig. 65B-1-001, Fig. 65B-1-002.	
3a	Unit cell parameters: Fig. 65B-1-003, Fig. 65B-1-004.	
5a, b	Dielectric constant: Fig. 65B-1-005, Fig. 65B-1-006; see also Effect of p and E_{bias} on κ_b' and tan δ: Fig. 65B-1-007, Fig. 65B-1-008, Fig. 65B-1-009, Fig. 65B-1-010, Fig. 65B-1-011. Phase diagram in regard to p: Fig. 65B-1-012. $d\Theta/dp$: Table 65B-1-001. Dielectric hysteresis loop: see	90Mae 96Kim, 96Man
14a	Bragg reflection: Fig. 65B-1-013.	

Table 65B-1-001. $(CH_3)_3NCH_2COO \cdot H_3(P_{1-x}As_x)O_4$ (BP–BA). Θ, $d\Theta/dp$ [94Lan]. Θ corresponds to Θ_a for x = 0…0.39, and to Θ_t for x = 1.

x	Θ [K]	$d\Theta/dp$ [K/MPa]
0 (BP)	86	–0.065
0.07	85	–0.066
0.24	79	–0.044
0.39	80	–0.059
1 (BA)	119	–0.045

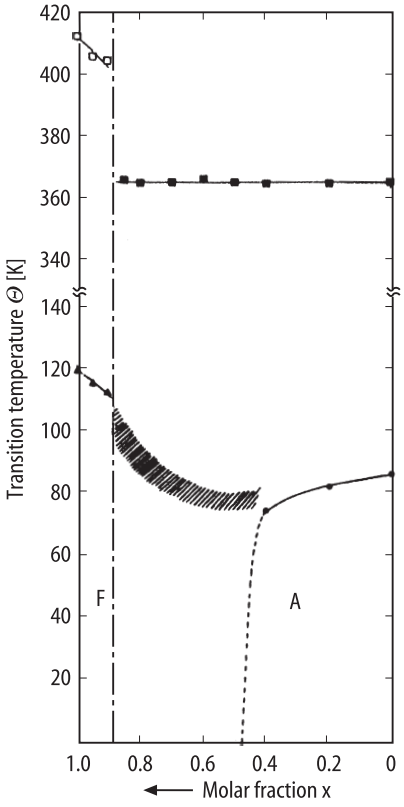

Fig. 65B-1-001. $(CH_3)_3NCH_2COO \cdot H_3(P_{1-x}As_x)O_4$ (BP–BA). Θ vs. x [89Mae]. Hatched area represents the temperature region where the dielectric constants show remarkable variations.

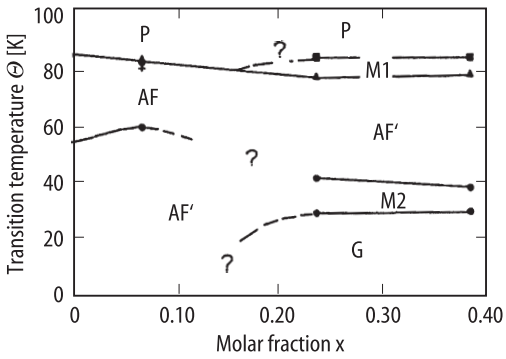

Fig. 65B-1-002. $(CH_3)_3NCH_2COO \cdot H_3(P_{1-x}As_x)O_4$ (BP–BA). Θ vs. x [94Lan]. P: paraelectric phase. AF, AF′: antiferroelectric phase. M1, M2: mixed phase. G: glassy phase.

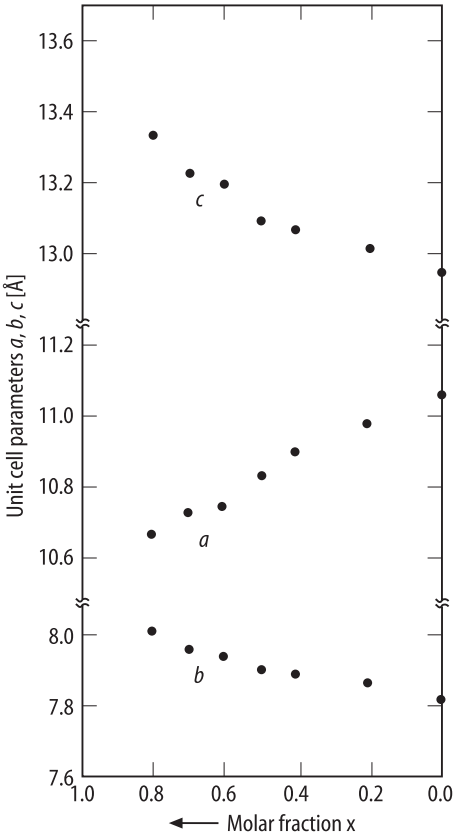

Fig. 65B-1-003. $(CH_3)_3NCH_2COO \cdot H_3(P_{1-x}As_x)O_4$ (BP–BA). *a*, *b*, *c* vs. x [89Mae]. *a*, *b*, *c*: unit cell parameters. T = RT.

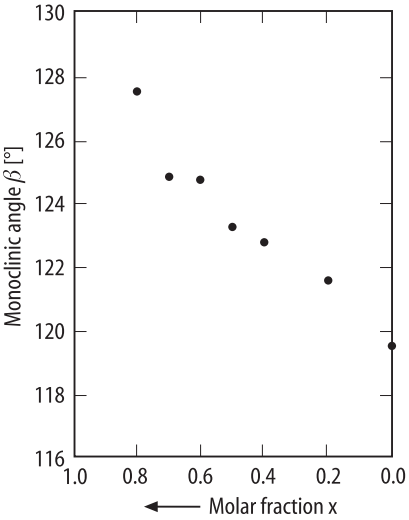

Fig. 65B-1-004. $(CH_3)_3NCH_2COO \cdot H_3(P_{1-x}As_x)O_4$ (BP–BA). β vs. x [89Mae]. β: monoclinic angle. T = RT.

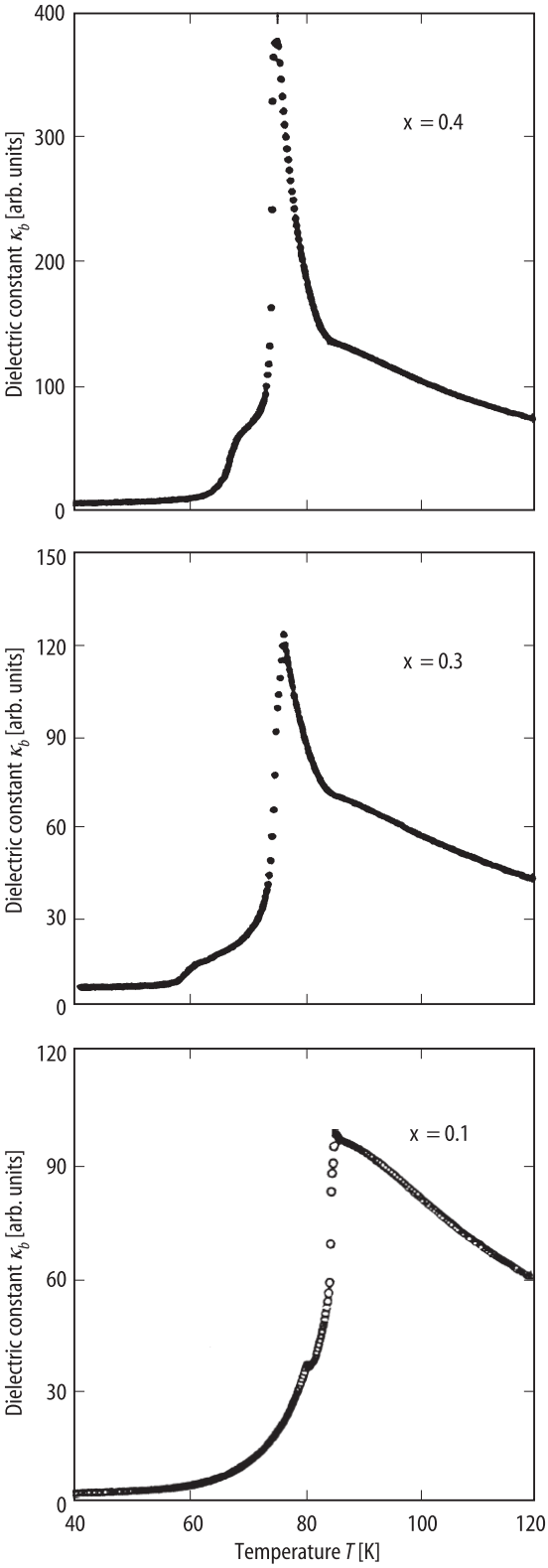

Fig. 65B-1-005. $(CH_3)_3NCH_2COO \cdot H_3(P_{1-x}As_x)O_4$ (BP–BA). κ_b vs. T [96Kim]. Parameter: x. Measured by a quasi-static method.

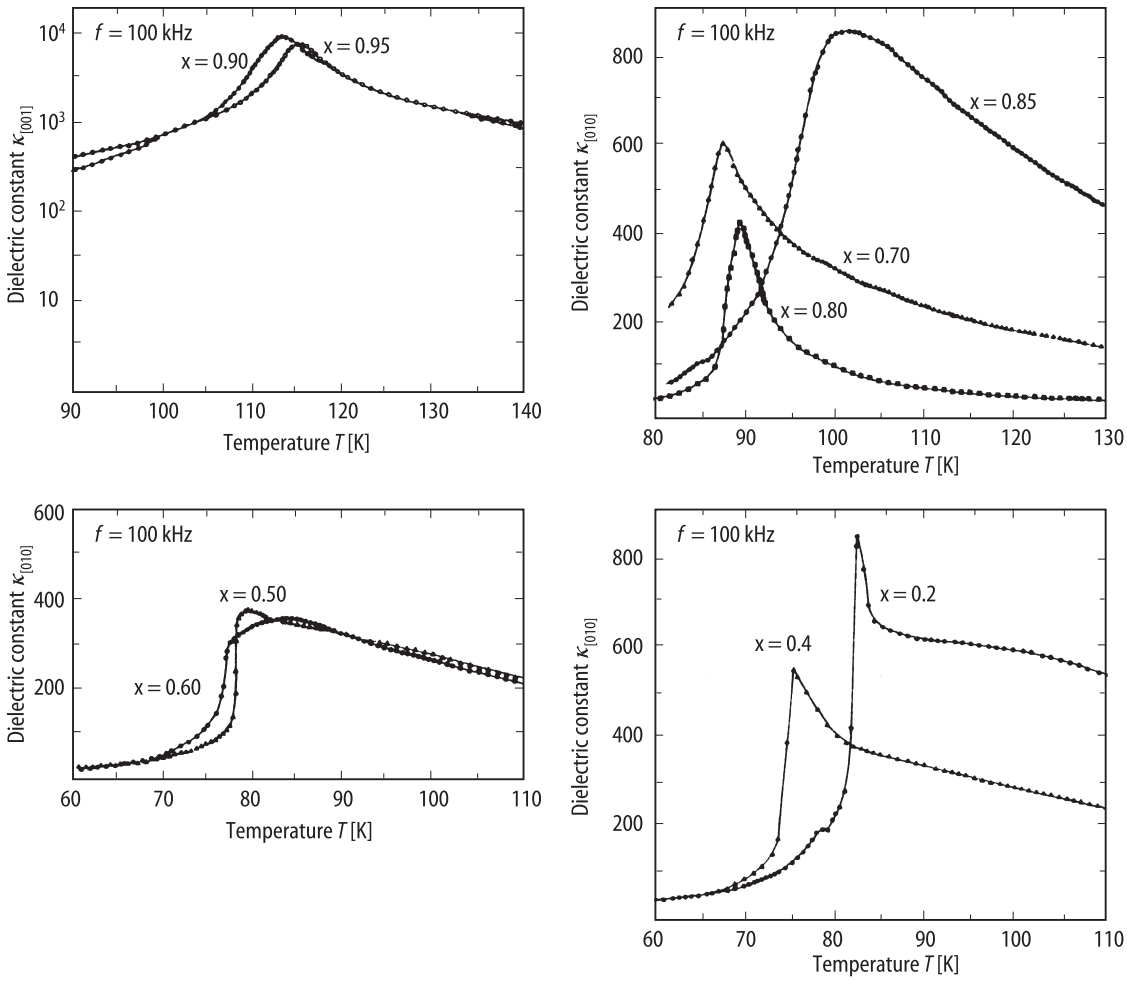

Fig. 65B-1-006. $(CH_3)_3NCH_2COO \cdot H_3(P_{1-x}As_x)O_4$ (BP–BA). $\kappa_{[010]}$, $\kappa_{[001]}$ vs. T [89Mae]. Parameter: x.

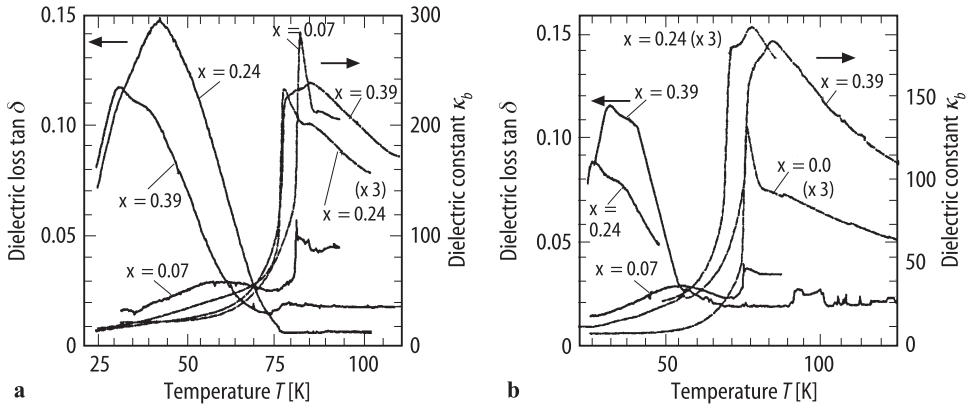

Fig. 65B-1-007. $(CH_3)_3NCH_2COO \cdot H_3(P_{1-x}As_x)O_4$ (BP–BA). κ_b, tan δ vs. T at (**a**) p = 10 MPa and (**b**) 100 MPa [94Lan]. Parameter: x.

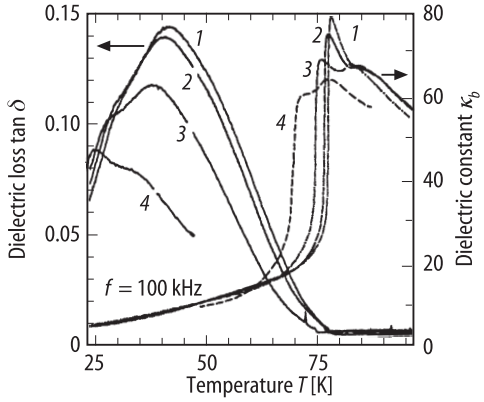

Fig. 65B-1-008. $(CH_3)_3NCH_2COO \cdot H_3(P_{0.76}As_{0.24})O_4$ (BP–BA). κ_b, tan δ vs. T [94Lan]. Parameter: p. Curve *1*: $p = 0$, *2*: 25 MPa, *3*: 75 MPa, *4*: 125 MPa.

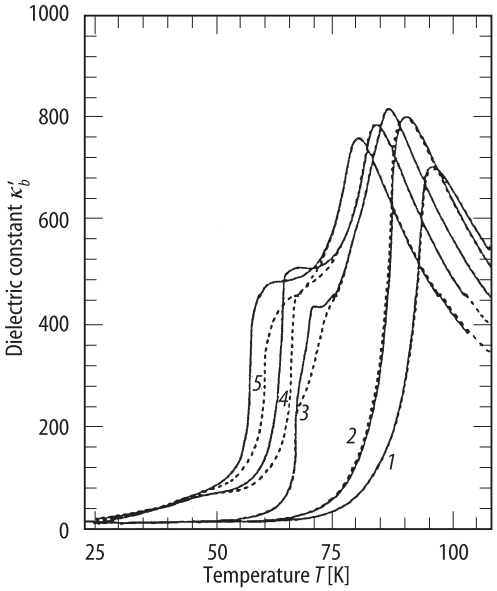

Fig. 65B-1-009. $(CH_3)_3NCH_2COO_3(P_{0.27}As_{0.73})O_4$ (BP–BA). κ'_b vs. T [96Man]. Parameter: p. Curve *1*: p = 8... 11 MPa, *2*: p = 60...75 MPa, *3*: p = 143...162 MPa, *4*: p = 237...262 MPa, *5*: p = 343...353 MPa. Full lines: on cooling, broken lines: on heating. f = 100 kHz.

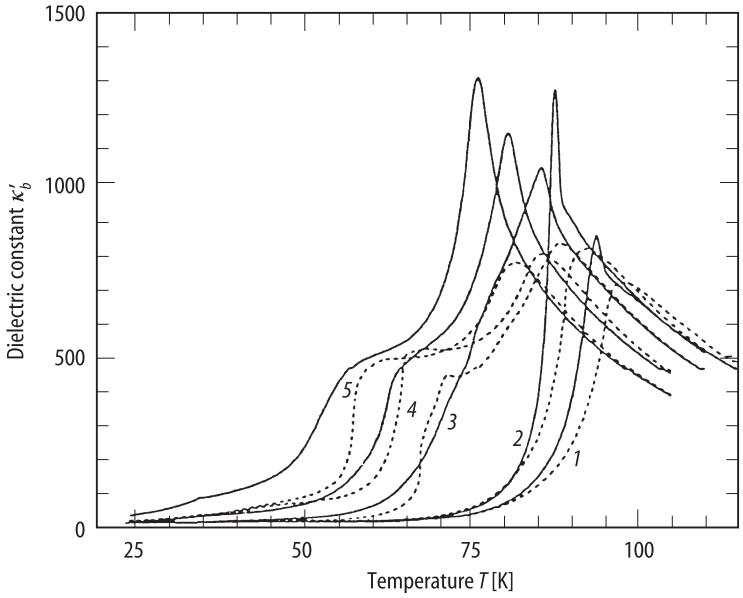

Fig. 65B-1-010. $(CH_3)_3NCH_2COO \cdot H_3(P_{0.27}As_{0.73})O_4$ (BP–BA). κ'_b vs. T [96Man]. Parameter: p, E_{bias}. Broken lines: $E_{bias} = 0$, full lines: $E_{bias} = 8.16 \cdot 10^5$ V m^{-1}. Curve *1*: $p \approx 10$ MPa, *2*: $p \approx 60$ MPa, *3*: $p \approx 150$ MPa, *4*: $p \approx 250$ MPa, *5*: $p \approx 350$ MPa. $f = 100$ kHz.

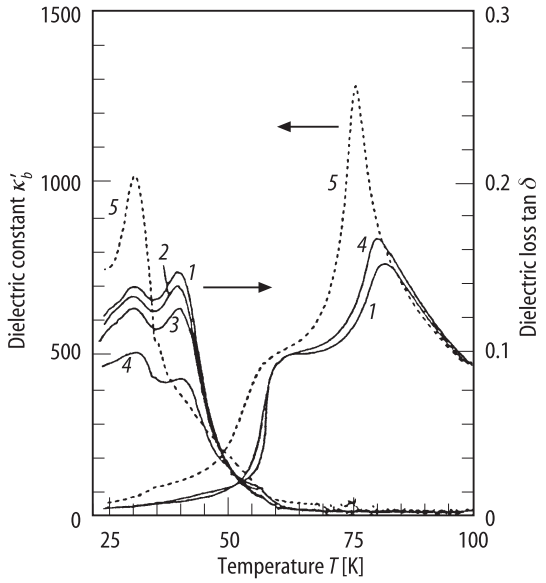

Fig. 65B-1-011. $(CH_3)_3NCH_2COO \cdot H_3(P_{0.27}As_{0.73})O_4$ (BP–BA). κ'_b, $\tan\delta$ vs. T [96Man]. Measured on cooling at $f = 100$ kHz, $p \approx 350$ MPa. Parameter: E_{bias}. Curve *1*: $E_{bias} = 0$, *2*: $1.02 \cdot 10^5$ V m^{-1}, *3*: $2.04 \cdot 10^5$ V m^{-1}, *4*: $4.08 \cdot 10^5$ V m^{-1}, *5*: $8.16 \cdot 10^5$ V m^{-1}.

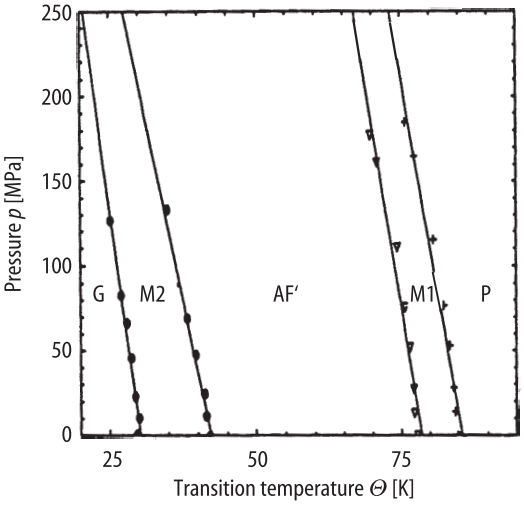

Fig. 65B-1-012. $(CH_3)_3NCH_2COO \cdot H_3(P_{0.76}As_{0.24})O_4$ (BP–BA). Θ vs. p [94Lan]. P: paraelectric phase. AF': antiferroelectric phase. M1, M2: mixed phases. G: glassy phase. See also Fig. 65B-1-002.

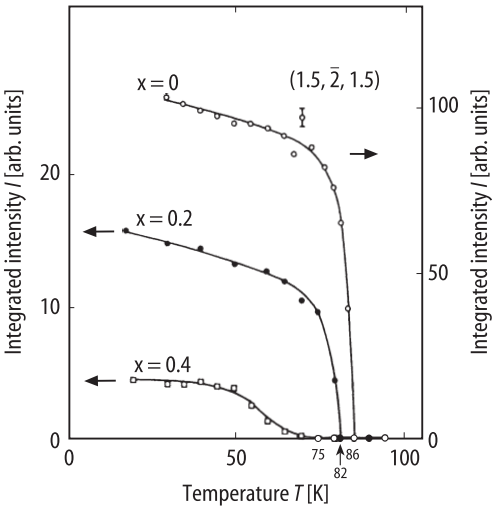

Fig. 65B-1-013. $(CH_3)_3NCH_2COO \cdot H_3(P_{1-x}As_x)O_4$ (BP–BA). $I_{(1.5,\ \bar{2}\ ,1.5)}$ vs. T [89Hay]. $I_{(1.5,\ \bar{2}\ ,1.5)}$: integrated intensity of X-ray superlattice reflection at $(1.5, \bar{2}, 1.5)$. Parameter: x.

References

89Hay Hayase, S., Koshida, T., Terauchi, H., Maeda, M., Suzuki, I.: Ferroelectrics **96** (1989) 221.
89Mae Maeda, M.: Ferroelectrics **96** (1989) 269.
90Mae Maeda, M., Suzuki, I.: Ferroelectrics **108** (1990) 351.
94Lan Lanceros-Méndez, S., Le Maire, M., Schaack, G., Schmitt-Lewen, M.: Ferroelectrics **157** (1994) 269.
96Kim Kim, Y.-H., Kim, B.-G., Kim, J.-J., Mochida, T., Miyajima, S.: J. Phys. Condens. Matter **8** (1996) 6095.
96Man Manger, M., Lanceros-Méndez, S., Schaack, G., Klöpperpieper, A.: J. Phys. Condens. Matter **8** (1996) 4617.

No. 65B-2 $(CH_3)_3NCH_2COO \cdot H_3PO_4$–$(CH_3)_3NCH_2COO \cdot H_3PO_3$ (BP–BPI)

1b	Θ vs. x phase diagram of $(CH_3)_3NCH_2COO \cdot H_3(PO_4)_{1-x}(PO_3)_x$: Fig. 65B-2-001; see also	95San
3a	Unit cell parameters: Fig. 65B-2-002, Fig. 65B-2-003.	
5a	Dielectric constant vs. temperature: Fig. 65B-2-004, Fig. 65B-2-005, Fig. 65B-2-006, Fig. 65B-2-007, Fig. 65B-2-008. Dielectric constant vs. frequency: Fig. 65B-2-009, Fig. 65B-2-010, Fig. 65B-2-011, Fig. 65B-2-012. Dielectric dispersion in γ-irradiated crystal: see Θ_p vs. x: see Fig. 65B-2-008.	96Ban1
c	Spontaneous polarization: Fig. 65B-2-013.	
d	Pyroelectric effect: see	90San, 93San
11	Electrical conductivity: Fig. 65B-2-014. For electrical conductivity of deuterated BP–BPI (x = 0.95), see	96Ban2
14a	Bragg reflection: see	95San

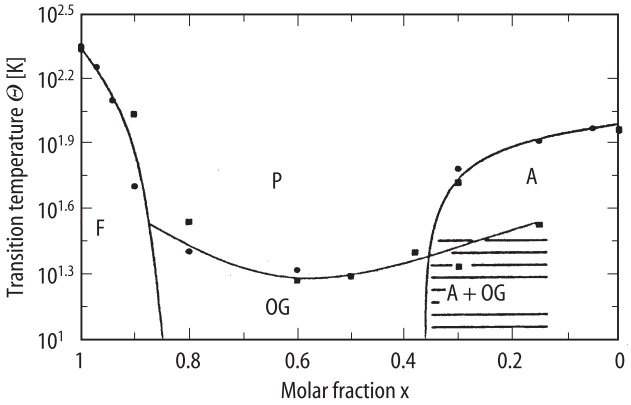

Fig. 65B-2-001. $(CH_3)_3NCH_2COO \cdot H_3(PO_4)_{1-x}(PO_3)_x$ (BP–BPI). Θ vs. x [96Rie]. P: paraelectric phase, F: ferroelectric phase, A: antiferroelectric phase, OG: orientational glass state. Hatched area: A + OG mixed phase. Full square: data in [96Rie], full circle: data taken from [90San, 93San].

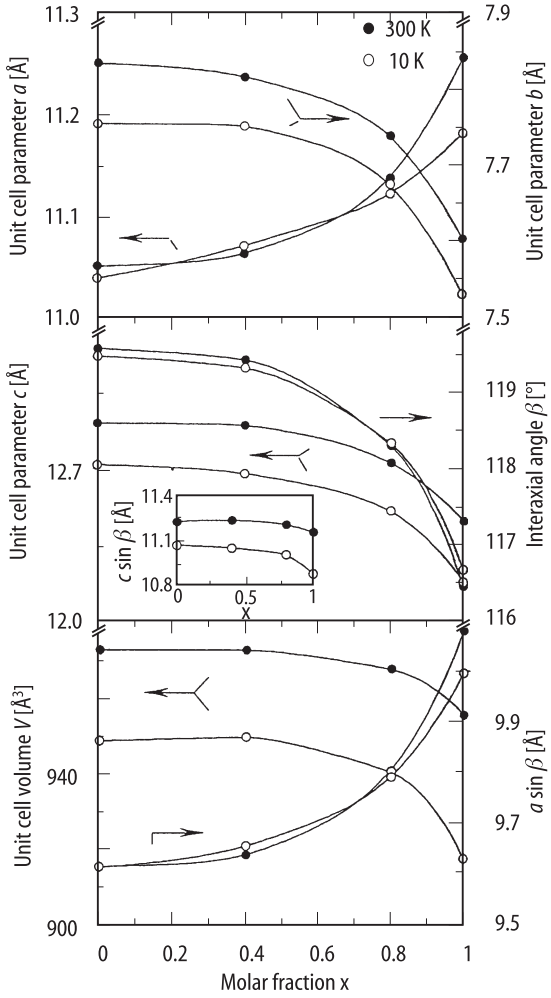

Fig. 65B-2-002. $(CH_3)_3NCH_2COO \cdot H_3(PO_4)_{1-x}(PO_3)_x$ (BP–BPI). a, b, c, β, V, $a \sin\beta$ vs. x [95San]. Parameter: T. V: unit cell volume. Insert: $c \sin\beta$ vs. x.

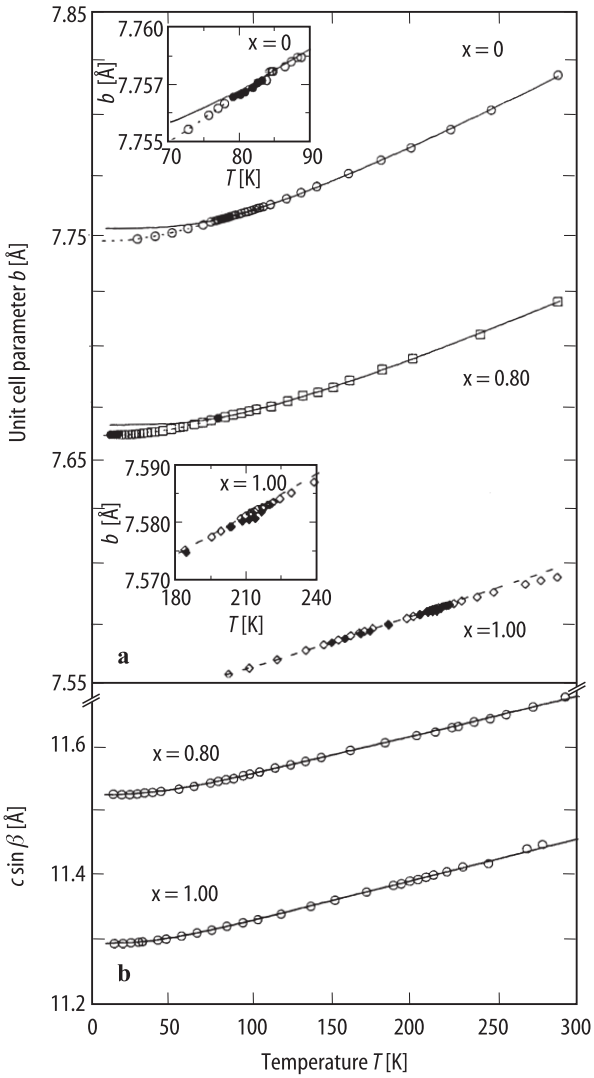

Fig. 65B-2-003. $(CH_3)_3NCH_2COO \cdot H_3(PO_4)_{1-x}(PO_3)_x$ (BP–BPI). (**a**) b vs. T, (**b**) $c \sin\beta$ vs. T [95San]. Parameter: x. Full squares for x = 1.0 are data on heating, others are on cooling. Full lines in (a) and (b) are results of fits to the Debye model, dashed lines in (a) are the other fits to the Debye model.

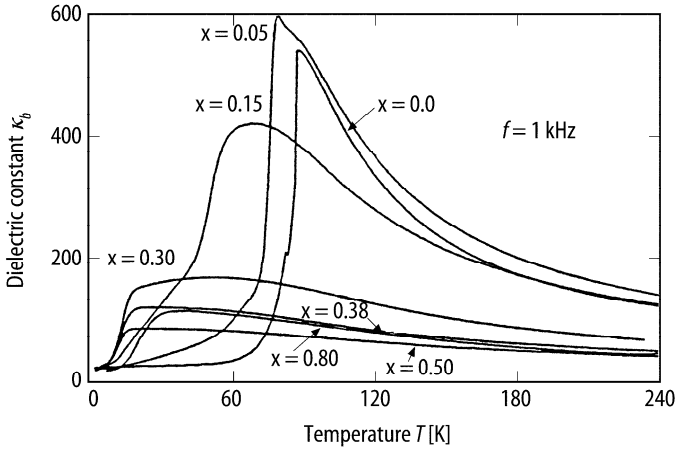

Fig. 65B-2-004. $(CH_3)_3NCH_2COO \cdot H_3(PO_4)_{1-x}(PO_3)_x$ (BP–BPI). κ_b vs. T [96Rie]. Parameter: x.

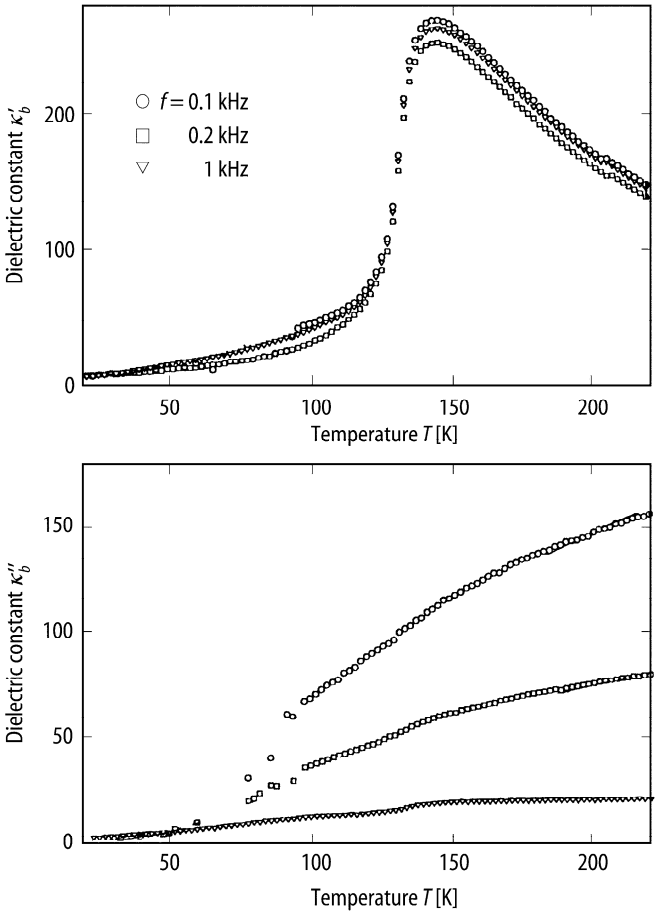

Fig. 65B-2-005. $(CH_3)_3NCH_2COO \cdot D_3(PO_4)_{0.95}(PO_3)_{0.05}$. κ_b', κ_b'' vs. T [96Ban2]. Parameter: f.

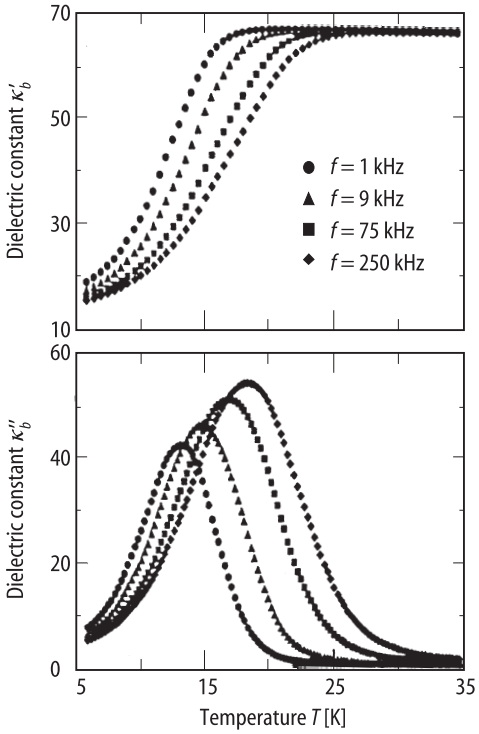

Fig. 65B-2-006. $(CH_3)_3NCH_2COO \cdot H_3(PO_4)_{0.50}(PO_3)_{0.50}$ (BP–BPI). κ_b', κ_b'' vs. T [96Rie]. Parameter: f.

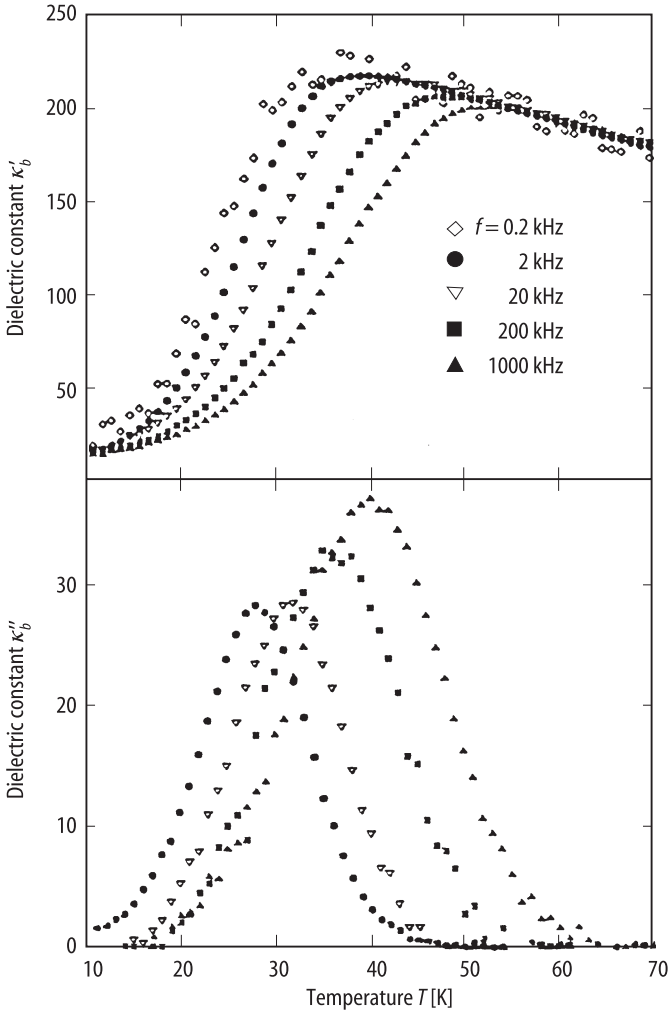

Fig. 65B-2-007. $(CH_3)_3NCH_2COO \cdot H_3(PO_4)_{0.15}(PO_3)_{0.85}$ (BP–BPI). κ_b', κ_b'' vs. T [94Ban]. Parameter: f.

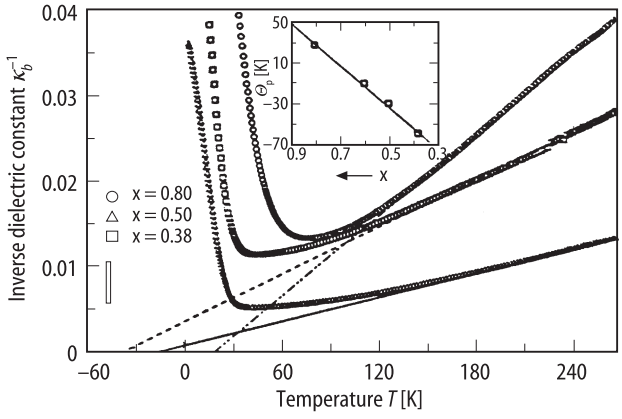

Fig. 65B-2-008. $(CH_3)_3NCH_2COO \cdot H_3(PO_4)_{1-x}(PO_3)_x$ (BP–BPI). κ_b^{-1} vs. T [96Rie]. Parameter: x. Insert: Θ_p vs. x. Θ_p: paraelectric Curie temperature.

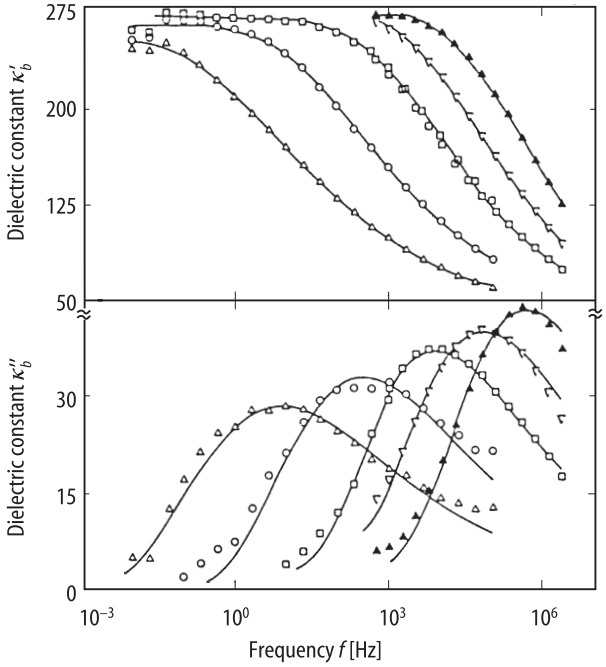

Fig. 65B-2-009. $(CH_3)_3NCH_2COO_3(PO_4)_{0.40}(PO_3)_{0.60}$ (BP–BPI). κ_b', κ_b'' vs. f [91Hut]. Parameter: T. Open upside triangle: T = 10.2K, open circle: 12.4 K, open square: 15.1 K, open downside triangle: 17.2 K, full upside triangle: 19.3 K.

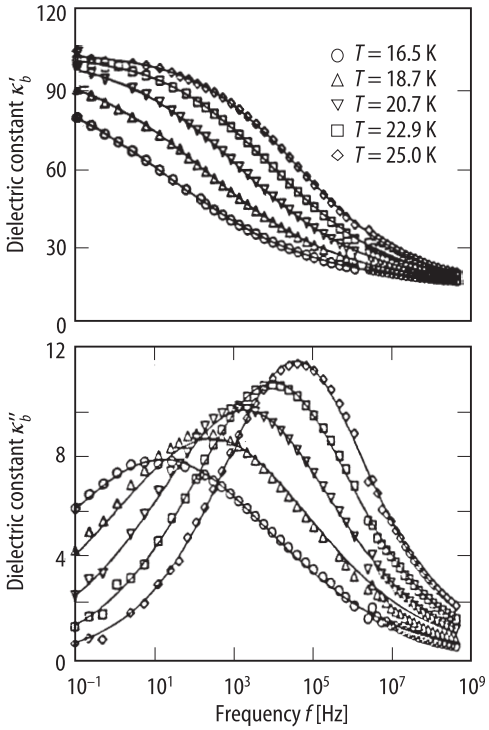

Fig. 65B-2-010. $(CH_3)_3NCH_2COO \cdot H_3(PO_4)_{0.20}(PO_3)_{0.80}$ (BP–BPI). κ_b', κ_b'' vs. f [96Rie]. Parameter: T. Full lines are fits using the Havriliak-Negami function.

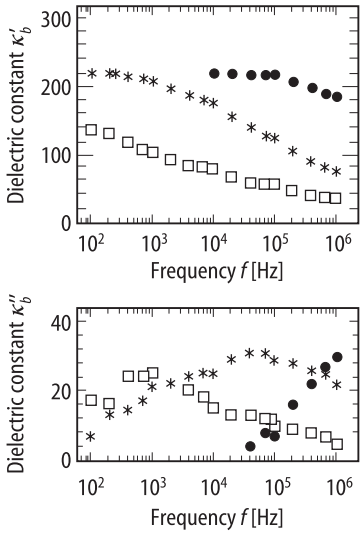

Fig. 65B-2-011. $(CH_3)_3NCH_2COO_3(PO_4)_{0.15}(PO_3)_{0.85}$ (BP–BPI). κ_b', κ_b'' vs. f [94Ban]. Parameter: T. Open square: $T = 24$ K, star: 32 K, full circle: 45 K.

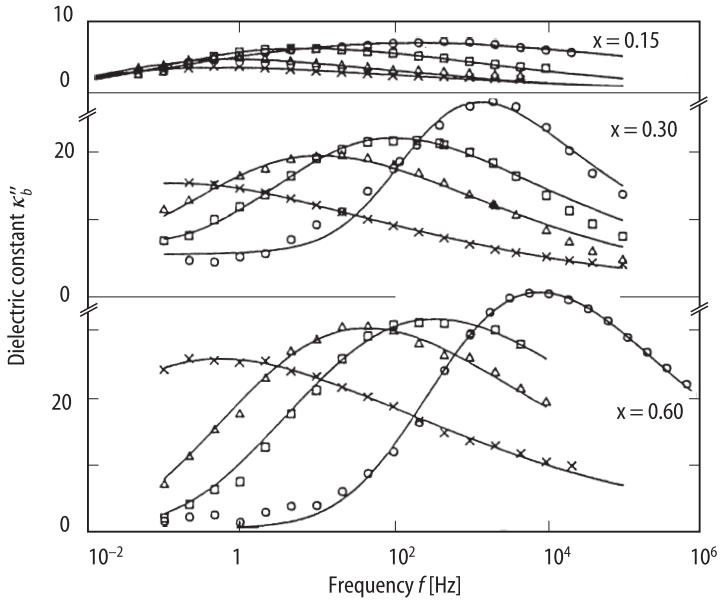

Fig. 65B-2-012. $(CH_3)_3NCH_2COO \cdot H_3(PO_4)_{1-x}(PO_3)_x$ (BP–BPI). κ_b'' vs. f [92Hut]. Parameter: x, T. Circle: $T = 15$ K, square: 13 K, triangle: 11 K, cross: 9 K.

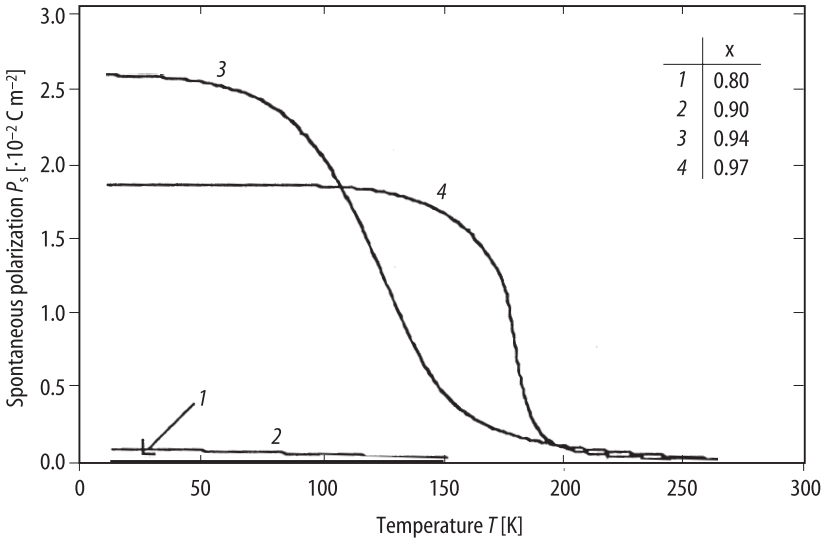

Fig. 65B-2-013. $(CH_3)_3NCH_2COO \cdot H_3(PO_4)_{1-x}(PO_3)_x$ (BP–BPI). P_s vs. T [93San]. Parameter: x. Obtained from pyroelectric current measurements.

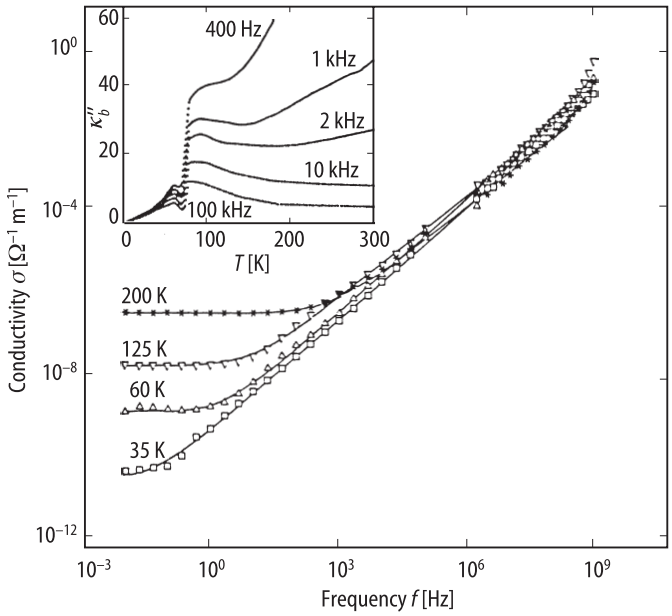

Fig. 65B-2-014. $(CH_3)_3NCH_2COO \cdot H_3(PO_4)_{0.95}(PO_3)_{0.05}$ (BP–BPI). σ vs. f [91Hut]. Parameter: T. σ: conductivity along the b axis. $\Theta_{III-II} = 79$ K. Insert: κ_b'' vs. T at various frequencies.

References

90San Santos, M.L., Azevedo, J.C., Almeida, A., Chaves, M.R., Pires, M.R., Müser, H.E., Albers, J.: Ferroelectrics **108** (1990) 363.

91Hut Hutton, S.L., Fehst, I., Böhmer, R., Braune, M., Mertz, B., Lunkenheimer, P., Loidl, A.: Phys. Rev. Lett. **66** (1991) 1990.

92Hut Hutton, S.L., Fehst, I., Böhmer, R., Loidl, A.: Ferroelectrics **127** (1992) 279.

93San Santos, M.L., Chaves, M.R., Almeida, A., Klöpperpieper, A., Müser, H.E., Albers, J.: Ferroelectrics Lett. **15** (1993) 17.

94Ban Banys, J., Klimm, C., Völkel, G., Bauch, H., Klöpperpieper, A.: Phys. Rev. B **50** (1994) 16751.

95San Santos, M.L., Kiat, J.M., Almeida, A., Chaves, M.R., Klöpperpieper, A., Albers, J.: Phys. Status Solidi (b) **189** (1995) 371.

96Ban1 Banys, J.B., Klimm, C., Völkel, G., Böttcher, R., Bauch, H.: J. Phys. Condens. Matter **8** (1996) L245.

96Ban2 Banys, J.B., Klimm, C., Völkel, G., Böttcher, R., Simon, J., Bauch, H., Klöpperpieper, A.: J. Phys. Condens. Matter **8** (1996) L681.

96Rie Ries, H., Böhmer, R., Fehst, I., Loidl, A.: Z. Phys. B **99** (1996) 401.